Single-Column Model Simulations
of Cloud Sensitivity to Forcing

A. D. Del Genio
National Aeronautics and Space Administration
Goddard Institute for Space Studies
New York, New York

A. B. Wolf
National Aeronautics and Space Administration
SGT, Inc., Goddard Institute for Space Studies
New York, New York

Introduction

The Atmospheric Radiation Measurement (ARM) Program single-column modeling (SCM) framework has to date used several fairly brief intensive observing periods (IOPs) to evaluate the performance of climate model parameterizations. With only a few weather events in each IOP, it is difficult to separate errors associated with the instantaneous dynamical forcing from errors in parameterization. It is also impossible to determine whether model errors are systematic and climatically significant. This ambiguity has hindered using SCMs to improve cloud parameterizations. For SCMs to become truly useful, they must be run for long periods of time, and they must be analyzed in ways that reveal how their parent 3-dimensional models might respond to changes in climate forcing.

The new continuous forcing dataset produced for the year 2000 by applying variational constraints to the rapid update cycle mesoscale model (Xie et al. 2003) offers the hope of significant progress. Initial comparisons with several ARM SCM IOP forcing datasets, by Xie et al., suggest that in seasons not dominated by deep convection at the Southern Great Plains (SGP) site, the continuous forcing product closely resembles the actual best estimate forcing derived from sondes and wind profilers. Thus, we have used the continuous forcing for the months of January, February, and March 2000, to drive the Goddard Institute for Space Studies (GISS) SCM. The SCM is run as a series of 24-hour forecasts that follow staggered 12-hour spinup periods from the observed state. The International Satellite Cloud Climatology Project (ISCCP) simulator software (Webb et al. 2001) is used to compare simulated cloud type occurrences to that observed by ISCCP for the same time period at the SGP.

Clouds at the SGP result from a variety of dynamic and thermodynamic conditions. In winter, especially, these can be thought of in terms of traditional baroclinic wave phases. Thus, we divide the ISCCP and SCM results into four dynamic "regimes" based on the sign of the large-scale 500 mb pressure vertical velocity ω and the instantaneous surface temperature anomaly T' (relative to the 3-month detrended mean). The regimes may be loosely interpreted as follows:

$\omega < 0$, T' > 0: warm front/warm sector region
$\omega < 0$, T' < 0: cold front/wraparound region
$\omega > 0$, T' < 0: post-cold front subsidence region
$\omega > 0$, T' > 0: high pressure/ridge crest region

The first two regions tend to be populated by high, thick clouds, while the last two regimes are dominated by low-level clouds.

Simply comparing observed and simulated clouds in the four regimes provides useful information on parameterization strengths and weaknesses, but it does not directly indicate whether the model will respond realistically to a climate perturbation. General circulation model (GCM) cloud responses to a climate forcing are likely to be associated with changes in the advection of heat and moisture that determine the instantaneous thermodynamic state of the column. The continuous forcing dataset is sufficiently long for us to find numerous examples of anomalous forcing that might serve as useful proxies for different types of climate change. For example, stronger/weaker than average moisture forcing might be relevant to upwelling/downwelling regions in an enhanced CO_2 world. By comparing ISCCP-observed and SCM-simulated cloud type anomalies in response to such anomalies in advective forcing, we hope to gain insights into the fidelity of the model's cloud feedback processes.

Vertical profiles of the mean temperature forcing and moisture forcing (Figure 1) show characteristic differences among the different dynamic regimes. Adiabatic cooling peaks near 400 mb in the upwelling regimes and is stronger in the cold front regime than the warm front regime. Adiabatic warming in the downwelling regimes is smaller in magnitude and has different vertical profiles, with a broad warming maximum behind the cold front and warming confined to the lower troposphere in high-pressure regions. Temperature forcing reverses sign at 300 mb in all regimes, perhaps a signature of sloping frontal surfaces. Advective moistening in the upwelling regimes peaks near 600-700 mb, while drying peaks at lower levels in the downwelling regimes. A double peak moisture forcing structure characterizes all regimes to some extent.

We vertically integrate the advective forcing profiles at each time step and scatter plot the resulting temperature forcing vs. moisture forcing values for different regimes. Figure 2 shows two examples, for the cold front/wraparound region (upper) and the post-cold front subsidence region (lower). For each dynamic regime we compute the mean temperature and moisture forcing and divide the population into 4 quadrants characterized by stronger than average T and q forcing (upper right), weaker than average T and q forcing (lower left), stronger T/weaker q forcing (upper left), and weaker T/stronger q forcing (lower right). For each quadrant we accumulate cloud type 2-dimensional histograms (cloud top pressure vs. optical thickness) and difference them with respect to the cloud type histograms for the regime mean, producing cloud type anomalies for a given type of anomalous advective forcing.

In some categories, anomalous advective forcing is mostly a change in forcing magnitude, with the vertical structure remaining fairly constant. A good example is the case of weaker than average T forcing, stronger than average q forcing for the cold front/wraparound region (not shown). The q forcing profiles for this case show some increase in altitude of the peak as forcing magnitude increases but the profile shapes do not change radically from case to case. In other categories, anomalous advective forcing behavior is more complex, for example for stronger than average T and q forcing in
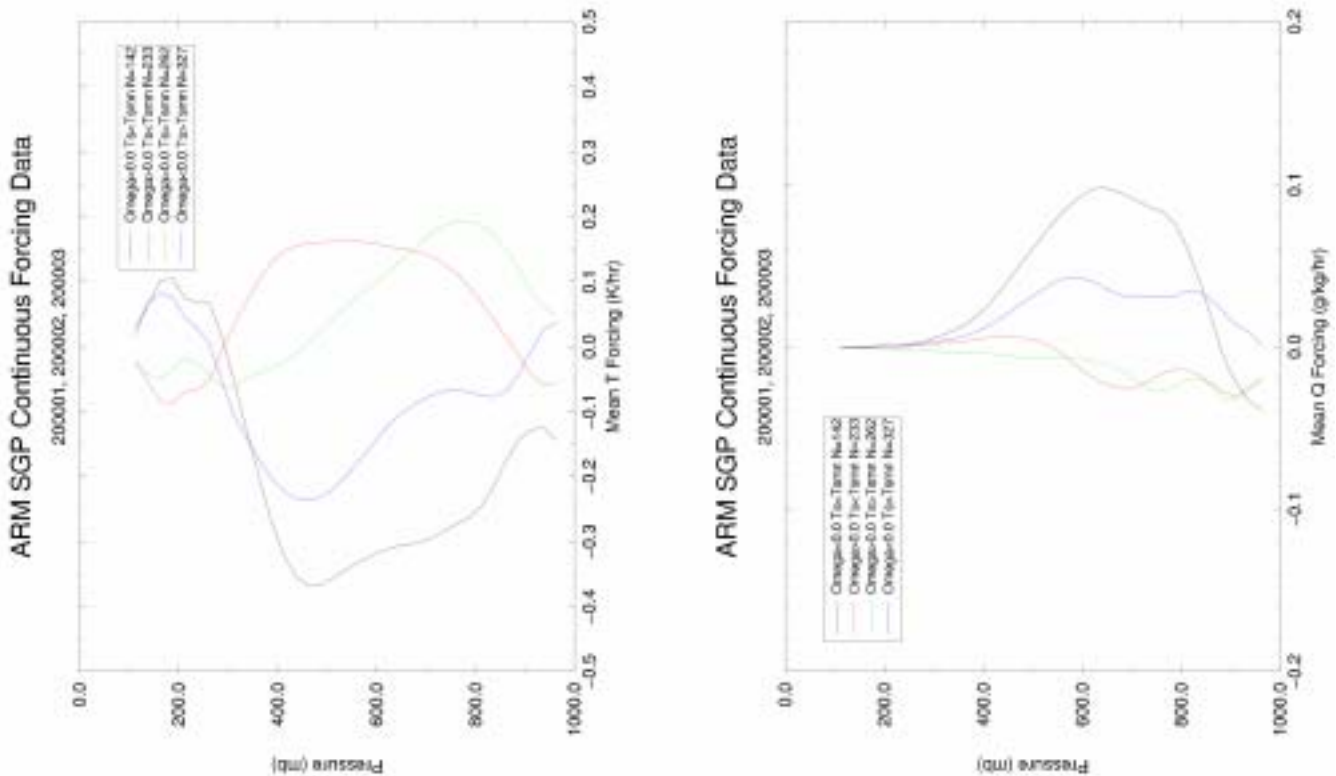
Figure 1. Mean vertical profiles of temperature forcing (upper) and moisture forcing (lower) for the SGP during January, February, and March 2000 composited by dynamic regime.

the post-cold front subsidence region. Individual profiles in this category can exhibit single or multiple peaks below the tropopause, at a variety of altitudes, and the location of peak forcing is not obviously related to the magnitude of the vertically integrated forcing. Such cases might be more difficult to relate to climate changes in any straightforward way.

Figure 3 shows cloud top pressure-optical thickness histograms in the post-cold front subsidence regime observed by ISCCP (left panels) and simulated by the SCM (right panels). The upper panels are mean histograms for the regime, while the lower panels are the anomalies under conditions of stronger than average T and q forcing. This regime is dominated by thick low/middle clouds and thin cirrus. The SCM has a similar cloud distribution, but with fewer cirrus and lower altitude low clouds. The tendency of GCMs to populate their lowest layers with clouds is well known. However, the ISCCP data have limitations as well. Wang et al. (1999) show that ISCCP cloud top pressures in the ASTEX region are biased low by ~60 mb on average due to errors near the inversion level in the input satellite-derived T and q profiles. A cloud radar version of the ISCCP simulator, currently being developed, would be especially valuable for this regime. The lower panels show that in both the real world and the SCM, strong forcing (greater adiabatic warming and drying) dissipates low cloud, and stronger adiabatic cooling near the tropopause increases thin cirrus. In this case, the model's cloud response is fairly realistic. Note that the model produces the correct cirrus response despite the absence of condensate transport; we believe that condensate transport is a secondary issue at best for SCMs.
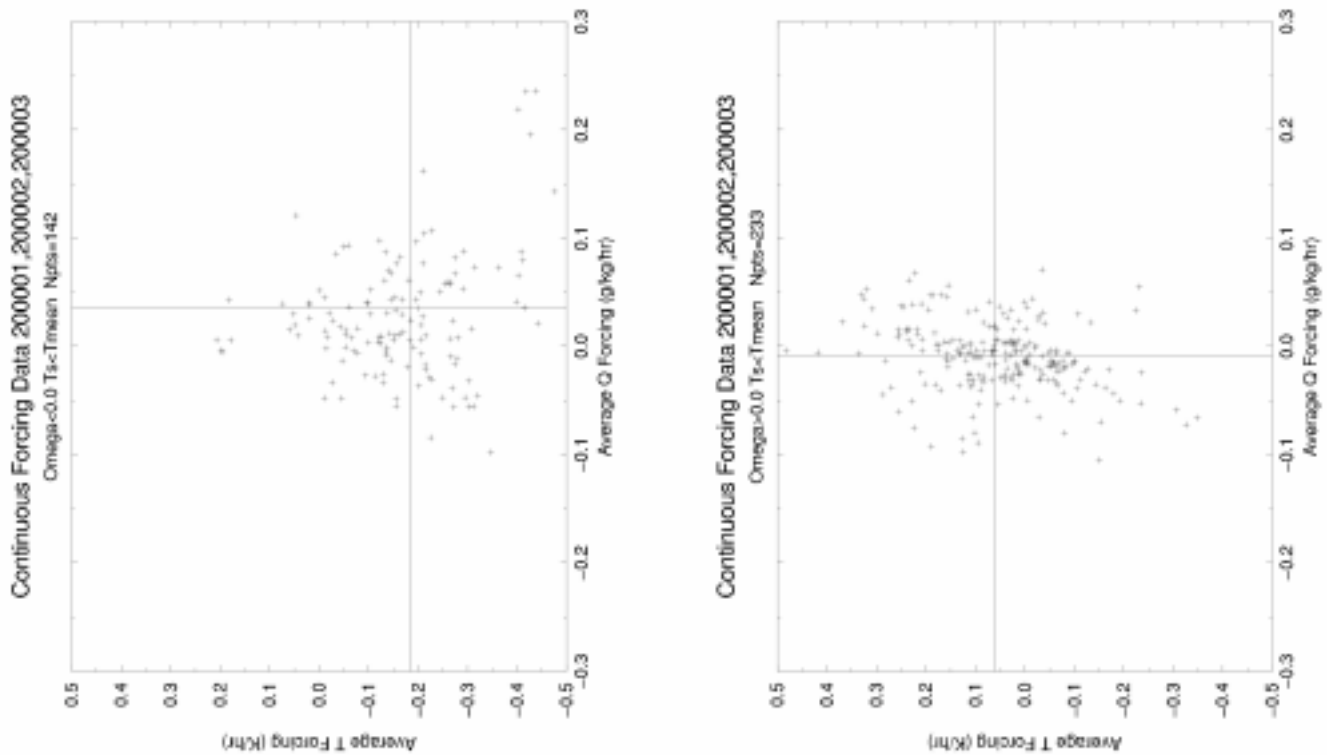
Figure 2. Scatter plots of vertically integrated temperature forcing vs. moisture forcing for the cold front/wraparound regime (upper) and the post-cold front subsidence regime (lower), illustrating the anomalous forcing definitions.

For the high pressure/ridge crest regime (not shown), the cloud type distribution is similar to that for the post-cold front regime, but with less low cloud and (in the data) some indication of descending cirrus cloud tops as the warm front approaches. The response of the real world and the SCM to stronger forcing is similar to the previous case except for the slight cirrus top lowering that the model does not capture. Low clouds do decrease in the data but by very small amounts.

For the warm front/warm sector regime (not shown), the cloud distribution is more complex. Four cloud types dominate the observations (1) thin high cirrus, (2) lower altitude cirrus, (3) deep convective cloud, and (4) low thick clouds. The mean cloud type distribution in the SCM is fairly similar. However, the model's response to stronger advective forcing differs in some ways from that observed. Both data and model show a positive cirrus response to stronger forcing. However, the data indicate an insignificant decrease in midlevel tops while the SCM produces a stronger midlevel cloud decrease. The data also indicate an insignificant decrease in low cloud, while the SCM predicts an increase in all low cloud types, for reasons that are not obvious. This would be a good target for a detailed model improvement study using individual cases.

Saving the worst for last, Figure 4 shows the histograms for the cold front/wraparound regime. In this regime the SCM likes to make deep convective clouds, midlevel very thick clouds, and thin cirrus, while the data show significantly less deep convective cloud and smaller optical thicknesses for the thick clouds that are present. It is conceivable that inadequacies in the continuous forcing contribute to these
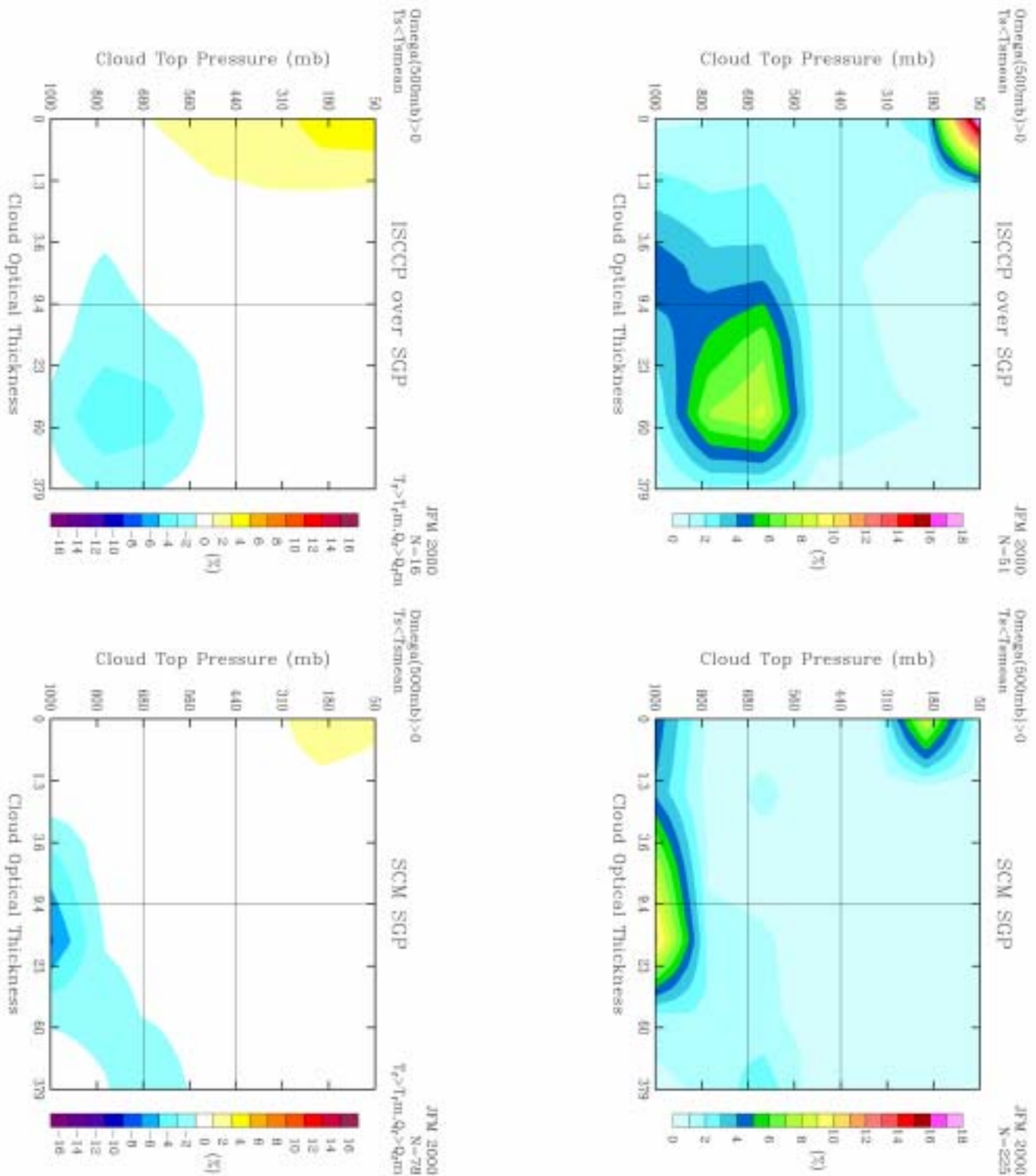
Figure 3. Cloud top pressure-optical thickness histograms observed by ISCCP (left panels) and simulated by the GISS SCM (lower panels) for the post-cold front subsidence regime. Upper panels show the mean histograms, while lower panels show the anomaly histograms for stronger than average temperature and moisture forcing.
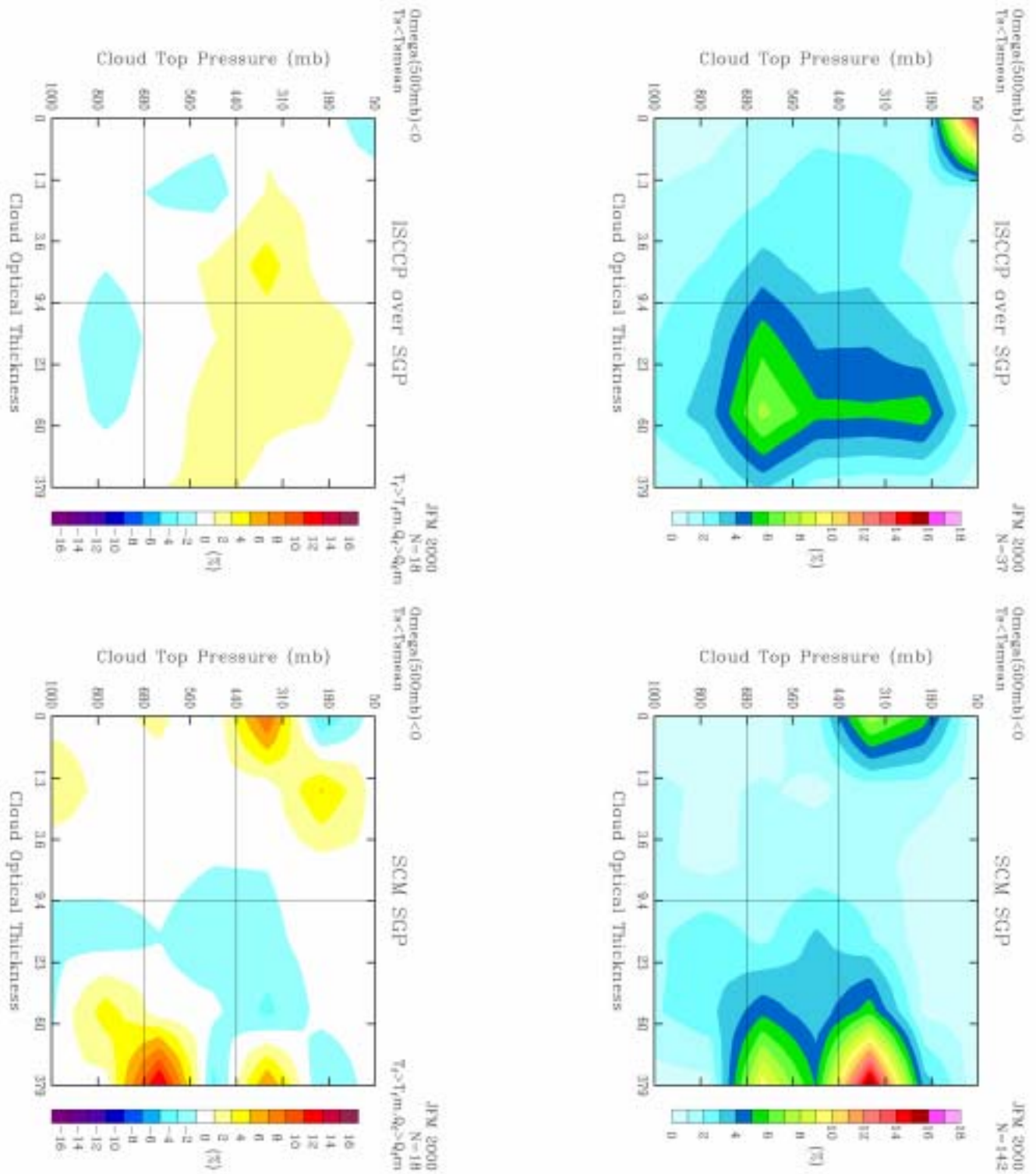
Figure 4. Same as in Figure 3 but for the cold front/wraparound regime.

errors, given the small spatial scales of frontal uplift, but we do not know this to be the case. The response of the model to stronger forcing in this regime could not be more unlike the real world. The data indicate primarily an upward shift in top altitudes of moderately thick clouds. The SCM produces a fairly random combination of cloud altitude and optical thickness changes that defies easy categorization. This is an example of the model behaving badly. For each of 16 anomaly situations (4 dynamical regimes x 4 combinations of stronger/weaker T and q forcing), we compute mean changes in high, middle, and low cloud cover. Figure 5 shows scatter plots of simulated vs. observed cloud cover change for each case, summarizing model cloud response performance in a variety of situations. For all three cloud types, the correlation between model and observed cloud response is ~0.6. The model generally produces the same sign of cloud response as observed when advective forcing anomalies are large, but there is some disagreement in the sign of cloud

Corresponding Author

Dr. Anthony D. Del Genio, adelgenio@giss.nasa.gov, (212) 678-5588

References

Wang, J., W. B. Rossow, T. Uttal, and M. Rozendaal, 1999: Variability of cloud vertical structure during ASTEX observed from a combination of rawinsonde, radar, ceilometer, and satellite. *Mon. Wea. Rev*., **127**, 2484-2502.

Webb, M., C. Senior, S. Bony, and J. J. Morcrette, 2001: Combining ERBE and ISCCP data to assess clouds in the Hadley Centre, ECMWF, and LMD atmospheric climate models. *Clim. Dyn*., **17**, 905-922.

Xie, S. C., R. T. Cederwall, J. J. Yio, and M. H. Zhang, 2003: Statistical study of SCM simulations using continuous forcing data derived from NWP products with the ARM data constraints. This Proceedings.
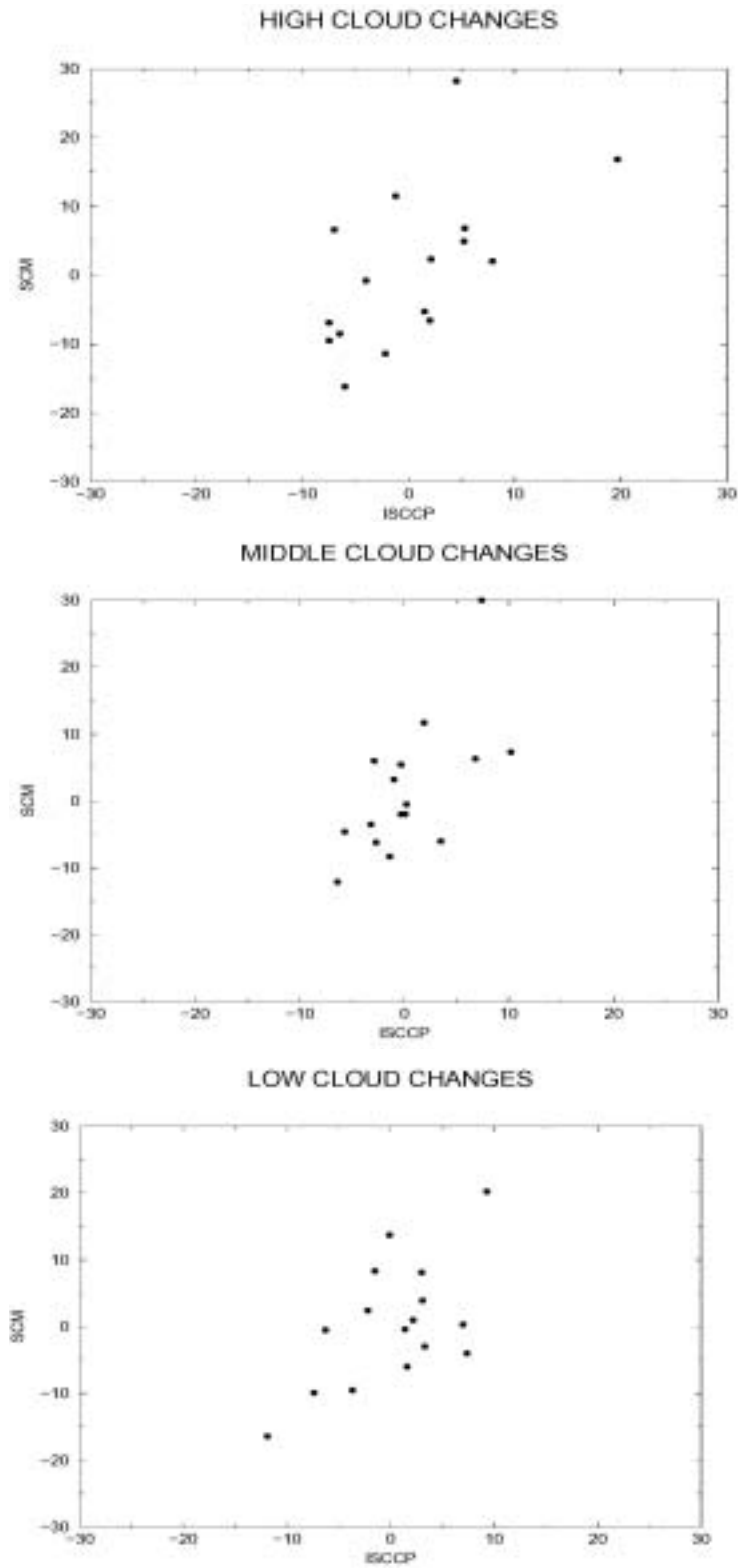
Figure 5. Scatter plots of SCM vs. ISCCP high (upper panel), middle (center panel), and low (lower panel) cloud cover for each of the 16 anomalous forcing categories.